Influence of electrode surface roughness and steric effects on the nonlinear electromechanical behavior of ionic polymer metal composites

Maurizio Porfiri*
Department of Mechanical and Aerospace Engineering, Polytechnic Institute of New York University, Brooklyn, New York 11201, USA
(Received 10 November 2008; published 27 April 2009)

In this paper, we analyze the influence of electrode surface roughness and steric effects on the nonlinear electromechanical behavior of ionic polymer metal composites (IPMCs). We use the modified Poisson-Nernst-Planck equations to describe the electric potential and mobile counterion distributions within the IPMC for a steady voltage applied across the IPMC rough electrodes. We present an analytical solution of the nonlinear three-dimensional boundary value problem based on the method of matched asymptotic expansions. The distribution of mobile counterions within the polymer region is characterized by thin boundary layers in the proximity to the polymer-electrode interfaces, where enrichment and depletion of mobile charges take place. The presence of rough landscapes drastically increases the polymer-electrode surfaces and thereby significantly improves the overall charge storage. We determine closed-form expressions for the average bending moment produced by the IPMC and for its average stored charge and capacitance. We show that the bending moment produced by an IPMC is linearly proportional to the stored charge, which in turn increases nonlinearly as the voltage applied across the electrodes increases. The average charge stored in the IPMC increases as the electrode surface roughness increases and decreases as steric effects become prominent.

DOI: 10.1103/PhysRevE.79.041503 PACS number(s): 82.45.Wx, 46.15.Ff, 68.35.Ct, 82.47.Gh

I. INTRODUCTION

Ionic polymer metal composites (IPMCs) are electroactive materials that can operate as sensors [1–4], actuators [5–12], and energy harvesting systems [13,14] in air and aqueous environments. An IPMC consists of an ion-exchange polymer membrane plated by noble metal electrodes and infused with a fluid solvent whose mobile counterions neutralize the fixed charges of the backbone polymer. Upon application of an electrical stimulus across the electrodes, the charge redistribution gives rise to a variety of concurrent microscopic effects. These effects result in charge storage at the electrodes and macroscopic mechanical bending. Conversely, a superimposed mechanical deformation induces charge storage at the electrodes and a voltage drop across them.

A variety of physics-based models have been proposed in the past few years to quantitatively describe the electromechanical response of IPMCs. In [15], linear irreversible thermodynamics is used to study IPMC actuation. In [5,16], a micromechanics framework is developed to characterize IPMC sensing and actuation. In [17], a phenomenological continuum model of IPMC actuation is proposed. In [7,18], multifield mixture theories are used to describe mechanical actuation and sensing of IPMCs. In [19–23], IPMC transduction is studied using a multifield chemoelectrical framework based on the Poisson-Nernst-Planck model.

Despite the largely different approaches followed in these modeling efforts, a general consensus on the driving phenomena of IPMC electromechanical behavior has been achieved (see, for example, [24]). These efforts have demonstrated that IPMC electromechanical behavior is primarily dictated by chemoelectric phenomena that take place in the proximity of the polymer-electrode interfaces. More specifically, it is now understood that IPMC response is mostly governed by double-layer effects at the polymer-electrode interfaces (see, for example, [25]) and that IPMC actuation is largely due to electrostatic pressure generated by local charge imbalance at the polymer-electrode interfaces. As documented in the electrochemistry literature (see, for example, [26–29]), double-layer phenomena are strongly affected by the geometry of the interfaces and rough landscapes may drastically alter double-layer capacitance and charge density. Rough electrodes have generally been observed in IPMCs in the form of deep metal protrusions in the polymer membrane [30–32]. In addition, experimental studies on IPMCs [30,31,33] have shown that electrode surface roughness is highly correlated with the IPMC giant capacitance that in turn prominently affects IPMC actuation performance. Nevertheless, most of the modeling efforts in the IPMC literature assume that the electrodes are perfectly flat surfaces (see, for example, [24]).

In this paper, we analyze the influence of the electrodes' surface roughness on the static nonlinear electromechanical behavior of IPMCs. We adopt the multifield chemoelectric framework originally proposed in [19–21] to determine the distribution of the electric potential and the concentration of the counterions in the backbone polymer region in response to a steady voltage difference applied across the IPMC rough electrodes. We extend the formulation of [19–21] to account for steric effects inevitably present at the polymer-electrode interfaces by considering the modified Poisson-Nernst-Planck model proposed in [34,35] for analyzing charge dynamics of electrolytes.

We use perturbation methods to determine a closed-form solution of the modified Poisson-Nernst-Planck model. In particular, we use the method of asymptotic expansions (see, for example, [36–38]) to determine a closed-form solution of the nonlinear boundary value chemoelectric problem. Matched asymptotic expansions have been successfully used in the analysis of symmetric binary electrolytes (see, for ex-

*mporfiri@poly.edu; http://faculty.poly.edu/~mporfiri/index.htm

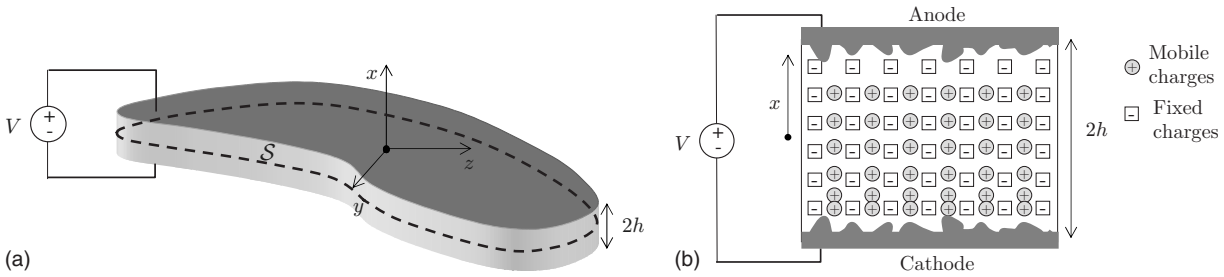

FIG. 1. Sketch of an IPMC illustrating (a) the problem geometry and coordinate system and (b) cation enrichment in the proximity of the cathode and cations depletion in the vicinity of the anode region.

ample, [34,35,39–41]). The application of matched asymptotic expansions to the analysis of IPMCs demands additional efforts due to the remarkable asymmetries in the voltage and charge distributions in the polymer region. Therefore, we build on the mathematical tools presented in [23] for studying charge dynamics of IPMCs in case of flat electrodes and in the absence of steric effects to develop a closed-form solution for the charge and electric potential distributions in case of rough landscapes and steric effects. Unlike the problem considered in [23], we focus on the static electromechanical response of IPMCs. In this case, the electric potential and mobile counterion concentration distributions at the leading order are constant in the bulk polymer region. While the mobile counterion concentration in the bulk polymer region is simply equal to the concentration of fixed charges, the numerical value of the electric potential is determined by asymptotic matching with the solution in the proximity of the electrodes. More specifically, we find that the electric potential in the bulk polymer region depends on the electrode morphology, the counterion packing limit, and the voltage applied across the IPMC electrodes.

The proposed solution allows for a quantitative understanding of double-layer effects in IPMCs in terms of the electrode surface roughness and the concentration steric limit. At the leading order, we transform the three-dimensional nonlinear boundary value problem into a handleable second-order ordinary differential equation with only initial conditions. We determine closed-form expressions for the charge stored in the IPMC and the average bending moment produced by the IPMC as a function of the electrode surface roughness and the packing limit of the counterion concentration. We show that the charge stored in the IPMC is independent of the IPMC thickness and nominal surface area, while it is strongly affected by the electrodes' surface area. The stored charge linearly increases with the electrode surface area and is reduced by steric effects. Further, we determine an analytical relationship between the charge stored in the IPMC and its bending moment. We show that the stored charge and the bending moment vary nonlinearly with the applied voltage. As the voltage increases, we find that the rate of change in the stored charge and bending moment decreases.

We organize the paper as follows. In Sec. II, we present the governing equation of the studied chemoelectric model. In Sec. III, we use the method of matched asymptotic expansions to determine the charge and electric potential distributions in the bulk polymer region (outer solution) and to formulate a handleable problem for the charge and concentration fields in the vicinity of the electrodes (inner problems). In Sec. IV, we present our results and compare our findings with available experimental results. Section V is left for conclusions.

II. PROBLEM STATEMENT

A. Modeling

We consider an IPMC comprised of a strip of an ion-conducting polymer membrane of nominal thickness $2h$ plated by two rough metallic electrodes and subjected to a voltage difference across the electrodes V (see Fig. 1). Points in the space are identified through the Cartesian coordinate system (x,y,z) in Fig. 1. The polymer region $\mathcal{P}$ is defined by

$$\mathcal{P}=\{(x,y,z):(y,z)\in\mathcal{S},\quad -h+\rho^{-}(y,z)\le x\le h-\rho^{+}(y,z)\},\tag{1}$$

where $\mathcal{S}$ is the polymer midsurface and the positive functions ρ^{+} and ρ^{-} describe the surface roughness of the anode and cathode regions, respectively. In other words, the magnitude of the functions ρ^{+} and ρ^{-} quantifies the through-the-thickness extension of the electrodes' metal protrusion in the bulk polymer region. The actual IPMC thickness at (y,z) is thus equal to $2h-[\rho^{+}(y,z)+\rho^{-}(y,z)]$. We partition the surface of the polymer region in the union of the polymer region mantle $\mathcal{M}$, the anode surface $\mathcal{S}^{+}$, and the cathode surface $\mathcal{S}^{-}$. Surface areas are indicated by $|\bullet|$. We assume that the functions $\rho^{\pm}$ satisfy

$$\int_{\mathcal{S}^{\pm}}\rho^{\pm}(y,z)d\mathcal{S}^{\pm}=0.\tag{2}$$

The surface element of the electrodes can be written in terms of the surface element of $\mathcal{S}$ as

$$d\mathcal{S}^{\pm}=d\mathcal{S}\sqrt{J^{\pm}(y,z)},\tag{3}$$

where we defined

$$J^{\pm}(y,z)=(1+\|\nabla_{s}\rho^{\pm}(y,z)\|^{2}).\tag{4}$$

The Jacobians in Eq. (4) measure the local surface change due to the electrode roughness. Here and henceforth, we decompose the three-dimensional nabla operator as $\nabla=\frac{\partial}{\partial x}\hat{i}+\nabla_{s}$, where ∇_{s} is the two-dimensional nabla operator in the yz plane and $\hat{i}$ is the unit vector along the x axis. Therefore, Eq. (2) can be rewritten as

$$\int_{\mathcal{S}} \rho^{\pm}(y,z)\sqrt{J^{\pm}(y,z)}dS = 0. \tag{5}$$

Thus, the nominal thickness $2h$ is defined so that the average of the surface roughness of the electrodes weighted by their surface area is zero.

We model the IPMC using the multifield chemoelectrical formulation proposed in [19–21]. Within this formulation, the IPMC kinematics is described by the concentration per unit hydrated polymer volume c of the mobile ion species and the electric potential field ψ in the polymer region. For ease of illustration, we assume that the mobile ionic species is positively charged. We further assume that both the fixed charges anchored to the backbone polymer and the mobile charges have valency equal to one.

The distribution of the electric potential in the polymer region is described by the Gauss law

$$\nabla \cdot \vec{D}(x,y,z) = F(c(x,y,z) - c_0), \tag{6}$$

F is Faraday's constant ($F=96\,485$ C mol^{-1}), c_0 is the concentration of the fixed ions, and $\vec{D}$ is the electric displacement vector. The electric displacement vector is related to the electric potential by

$$\vec{D}(x,y,z) = -\varepsilon_0\varepsilon_r \nabla \psi(x,y,z), \tag{7}$$

where ε_0 is the vacuum permittivity ($\varepsilon_0=8.8542\times10^{-12}$ F m^{-1}) and ε_r is the hydrated polymer dielectric constant. Substituting Eq. (7) into Eq. (6), we find the Poisson equation

$$-\varepsilon_0\varepsilon_r \Delta \psi(x,y,z) = F(c(x,y,z) - c_0), \tag{8}$$

where Δ is the Laplace operator.

We use the model proposed in [34,35] to account for steric effects. Under static conditions, this model provides the following relation between the concentration c and the electric potential ψ:

$$\frac{c_0}{c_0 - \nu c(x,y,z)} \nabla c(x,y,z) + \frac{F}{RT} c(x,y,z) \nabla \psi(x,y,z) = 0, \tag{9}$$

where R is the universal gas constant ($R=8.3143$ J mol^{-1} K^{-1}), T is the IPMC temperature, and ν is a dimensionless positive parameter smaller than 1 that measures the concentration packing limit. If $\nu=0$, mobile counterions can indefinitely grow in the polymer region. If $0<\nu<1$, the largest concentration of mobile counterions is bounded by c_0/ν. Following the argument of [34,35], the maximum concentration c_0/ν can be expressed as $c_0/\nu = a^{-3}/N$, where N is the Avogadro's number (6.0221×10^{23} mol^{-1}) and a is a typical spacing between the charged ions that is not smaller than the ionic radius (generally ≈ 1 Å). For typical IPMCs (see, for example, [20,21]) $c_0 \approx 1000$ mol m^{-3}. This implies that ν varies in the broad range of $6\times10^{-4}-0.2$ as a changes in the range of 1–7 Å examined in [34,35] to include relevant physical effects, such as ion-ion correlation.

Equations (8) and (9) describe the charge and electric potential distributions in IPMCs under static conditions. We assume that the IPMC is electroneutral, the electrodes are perfect conductors, and fringing electric fields at the polymer mantle are negligible. We further discard Stern layers and redox reactions at the polymer-electrode interfaces. Therefore, we consider the following set of boundary and integral conditions:

$$\int_{\mathcal{P}} [c(x,y,z) - c_0] d\mathcal{P} = 0, \tag{10a}$$

$$\psi(\pm(h-\rho^{\pm}),y,z) = \pm\frac{V}{2}, (y,z) \in \mathcal{S}, \tag{10b}$$

$$\nabla_s \psi(x,y,z) \cdot \hat{n}_{\mathcal{M}}(y,z) = 0, (x,y,z) \in \mathcal{M}, \tag{10c}$$

where we used $\hat{n}_{(\bullet)}$ to identify the unit outward normal vector to the surface $(\bullet)$. More specifically, Eq. (10a) implies that the IPMC is globally electroneutral, Eq. (10b) imposes that the voltage difference across the IPMC electrode is V, and Eq. (10c) forces the electric field to be directed along the through-the-thickness direction at the polymer mantle.

The charge per unit interface-surface stored in each electrode, say $q_{\star}^{\pm}$, is given by the jump of the normal component of the electric displacement vector across the polymer-electrode interface, that is,

$$q_{\star}^{\pm}(y,z) = \mp \vec{D}(\pm(h-\rho^{\pm}(y,z)),y,z) \cdot \hat{n}_{\mathcal{S}^{\pm}}(y,z). \tag{11}$$

Thus, the charge surface density in the anode and cathode regions per unit nominal surface, say $q^{\pm}$, can be written as

$$q^{\pm}(y,z) = \pm\varepsilon_0\varepsilon_r \left(\frac{\partial \psi(x,y,z)}{\partial x} \pm \nabla_s \psi(x,y,z) \cdot \nabla_s \rho^{\pm}(y,z) \right) \Bigg|_{x=\pm(h-\rho^{\pm}(y,z))}, \tag{12}$$

where we used Eq. (3) and

$$\hat{n}_{\mathcal{S}^{\pm}}(y,z) = \pm\frac{1}{\sqrt{J^{\pm}(y,z)}}[\hat{i} \pm \nabla_s \rho^{\pm}(y,z)]. \tag{13}$$

By integrating Eq. (6) in $\mathcal{P}$ and by using the divergence theorem and Eqs. (10a) and (10c), we find

$$\int_{\mathcal{S}} q^{+}(y,z) d\mathcal{S} + \int_{\mathcal{S}} q^{-}(y,z) d\mathcal{S} = 0. \tag{14}$$

We note that Eqs. (10c) and (14) imply the global electroneutrality condition (10a). Further, Eq. (14) indicates that the net charge stored in the anode is equal to the net charge stored in the cathode. We refer to the charge stored in the anode per unit nominal surface area as Q, that is, we define

$$Q = \frac{\varepsilon_0 \varepsilon_r}{|\mathcal{S}|} \times \int_{\mathcal{S}} \left(\frac{\partial \psi(x,y,z)}{\partial x} + \nabla_s \psi(x,y,z) \cdot \nabla_s \rho^+(y,z) \right) \Big|_{x=h-\rho^+(y,z)} d\mathcal{S}. \tag{15}$$

Following [5,16], the electrostatic pressure in the polymer region can be related to the charge imbalance through

$$\sigma(x,y,z) = kF(c(x,y,z) - c_0), \tag{16}$$

where the constant k is related to the microstructure of the polymer and to its hydration level. The bending moment with respect to the yz plane induced by the electrostatic pressure on the IPMC at (y,z) is (see, for example, [42,43])

$$m(y,z) = -\int_{-h+\rho^-(y,z)}^{h-\rho^+(y,z)} x\sigma(x,y,z)dx. \tag{17}$$

We measure the overall actuation performance of the IPMC through the average bending moment defined by

$$M = \frac{1}{|\mathcal{S}|}\int_{\mathcal{S}} m(y,z)d\mathcal{S} \equiv -\frac{1}{|\mathcal{S}|}\int_{\mathcal{P}} x\sigma(x,y,z)d\mathcal{P}. \tag{18}$$

By substituting Eq. (8) into Eq. (18), integrating by parts, and using the divergence theorem and the boundary conditions (10), we find

$$M = \varepsilon_0 \varepsilon_r \frac{k}{|\mathcal{S}|}\left(\int_{\mathcal{S}^+} x \nabla \psi(x,y,z) \cdot \hat{n}_{\mathcal{S}^+}(y,z) d\mathcal{S}^+ + \int_{\mathcal{S}^-} x \nabla \psi(x,y,z) \cdot \hat{n}_{\mathcal{S}^-}(y,z) d\mathcal{S}^- - \int_{\mathcal{P}} \frac{\partial \psi(x,y,z)}{\partial x} d\mathcal{P} \right). \tag{19}$$

By substituting Eqs. (3), (10b), and (13) into Eq. (19) and by accounting for Eq. (12), we have

$$M = -\varepsilon_0 \varepsilon_r kV + 2khQ - \frac{k}{|\mathcal{S}|}\int_{\mathcal{S}} [q^+(y,z)\rho^+(y,z) - q^-(y,z)\rho^-(y,z)]d\mathcal{S}. \tag{20}$$

We note that the average bending moment does not change when computed with respect to different planes that are orthogonal to the x axis. Further, if $\rho^{\pm}=0$, that is, in case of flat electrode, the last summand in the right-hand side of Eq. (20) is zero.

B. Nondimensional governing equations

We nondimensionalize the electric potential ψ with respect to the so-called thermal voltage RT/F and we nondimensionalize the counterion concentration with respect to the fixed charges concentration c_0. Moreover, we select the polymer nominal semithickness h as the characteristic length for scaling x, y, and z. Through nondimensionalization, the governing Eqs. (8) and (9) become

$$-\delta^2 \tilde{\Delta}\tilde{\psi}(\tilde{x},\tilde{y},\tilde{z}) = \tilde{c}(\tilde{x},\tilde{y},\tilde{z}) - 1, \tag{21a}$$

$$\frac{1}{1-\nu\tilde{c}}\tilde{\nabla}\tilde{c}(\tilde{x},\tilde{y},\tilde{z}) + \tilde{c}(\tilde{x},\tilde{y},\tilde{z})\tilde{\nabla}\tilde{\psi}(\tilde{x},\tilde{y},\tilde{z}) = 0, \tag{21b}$$

where the dimensionless variables and operators are indicated with a superimposed tilde, that is, $(\tilde{x},\tilde{y},\tilde{z})=(x,y,z)/h$, $\tilde{\psi}=\psi/(RT/F)$, $\tilde{c}=c/c_0$, $\tilde{\nabla}=\nabla/h$, and $\tilde{\Delta}=\Delta/h^2$. Further, we defined

$$\delta = \frac{\lambda}{h}, \tag{22}$$

where λ is the so-called Debye screening length (see, for example, [39]) that is given by

$$\lambda = \frac{1}{F}\sqrt{\frac{\varepsilon_0 \varepsilon_r RT}{c_0}} \tag{23}$$

For commonly studied ionic membranes (see, for example, [20,21]), $c_0 \approx 1000$ mol m^{-3}, $h \approx 10^{-4}$ m, and $\varepsilon_r \approx 10-100$. Therefore, at room temperature, $\lambda \approx 1-10$ Å and $\delta \approx 10^{-6}-10^{-5}$. We note that electrochemical systems characterized by comparable values of Debye screening lengths, typically low temperature or highly concentrated solutions, have been successfully studied in the continuum limit given by the Poisson-Nernst-Planck model (see, for example, [25]). The continuum modeling approach based on the Poisson-Nernst-Planck equation set is capable of reliably predicting important macroscopic quantities, such as average current and voltage, even when the spatial extent of the system is comparable with the ion size [44], such as narrow ion channel. A detailed discussion of the limitations of the Poisson-Nernst-Planck system in analyzing ion channels can be found in [44,45] along with alternative approaches based on Brownian dynamics, Monte Carlo simulations, and refined continuum theories.

The dimensionless form of the boundary and integral conditions (10b), (10c), and (14) is

$$\tilde{\psi}(\pm(1-\tilde{\rho}^{\pm}(\tilde{y},\tilde{z})),\tilde{y},\tilde{z}) = \pm\frac{\alpha}{2}, (\tilde{y},\tilde{z}) \in \tilde{\mathcal{S}}, \tag{24a}$$

$$\tilde{\nabla}_s\tilde{\psi}(\tilde{x},\tilde{y},\tilde{z}) \cdot \hat{n}_{\mathcal{M}}(\tilde{y},\tilde{z}) = 0, \quad (\tilde{x},\tilde{y},\tilde{z}) \in \tilde{\mathcal{M}}, \tag{24b}$$

$$\int_{\tilde{\mathcal{S}}} \left(\frac{\partial \tilde{\psi}(\tilde{x},\tilde{y},\tilde{z})}{\partial \tilde{x}} + \tilde{\nabla}_s\tilde{\psi}(\tilde{x},\tilde{y},\tilde{z}) \cdot \tilde{\nabla}_s\tilde{\rho}^+(\tilde{y},\tilde{z}) \right) \Big|_{\tilde{x}=(1-\tilde{\rho}^+(\tilde{y},\tilde{z}))} d\tilde{\mathcal{S}} = \int_{\tilde{\mathcal{S}}} \left(\frac{\partial \tilde{\psi}(\tilde{x},\tilde{y},\tilde{z})}{\partial \tilde{x}} - \tilde{\nabla}_s\tilde{\psi}(\tilde{x},\tilde{y},\tilde{z}) \cdot \tilde{\nabla}_s\tilde{\rho}^-(\tilde{y},\tilde{z}) \right) \Big|_{\tilde{x}=-(1-\tilde{\rho}^-(\tilde{y},\tilde{z}))} d\tilde{\mathcal{S}}, \tag{24c}$$

where $\tilde{\rho}^{\pm}=\rho^{\pm}/h$ is the dimensionless electrode roughness, $\tilde{\mathcal{S}}$ is the scaled polymer midsurface, $\tilde{\mathcal{M}}$ is the scaled polymer mantle, and $\alpha=FV/(RT)$ is the dimensionless voltage applied across the electrodes. The dimensionless forms of the Jacobians $\tilde{J}^{\pm}$ are defined by $\tilde{J}^{\pm}(\tilde{y},\tilde{z})=J^{\pm}(y,z)$.

III. MATCHED ASYMPTOTIC EXPANSIONS

Here, we derive an analytical solution for the concentration and electric potential in the IPMC by using the method of matched asymptotic expansions. Our study is limited to the leading-order solution of the modified Poisson-Nernst-Planck model. Consistently, with related studies on symmetric binary electrolytes (see, for example, [26,27]), we find that the leading-order solution is sensitive to any minute change in the local electrode local morphology, that is, the concentration boundary layer fully adhere to the rough electrodes. The validity of this solution is limited to the case in which the electrode characteristic planar length, which measures the smallest wavelength of roughness changes [26,27], is considerably larger than the Debye screening length that instead estimates the boundary layers' extent. In other words, the leading-order solution describes the IPMC physics in case the electrodes are locally flat with respect to the Debye screening length that practically sets the scale of the electrode roughness.

A. Outer expansion: Polymer bulk region

We seek regular asymptotic expansions of the electric potential and concentration in the outer region, that is,

$$\tilde{\psi}^o(\tilde{x},\tilde{y},\tilde{z}) = \tilde{\psi}_0^o(\tilde{x},\tilde{y},\tilde{z}) + \delta\tilde{\psi}_1^o(\tilde{x},\tilde{y},\tilde{z}) + \delta^2\tilde{\psi}_2^o(\tilde{x},\tilde{y},\tilde{z}) + \cdots, \tag{25a}$$

$$\tilde{c}^o(\tilde{x},\tilde{y},\tilde{z}) = \tilde{c}_0^o(\tilde{x},\tilde{y},\tilde{z}) + \delta\tilde{c}_1^o(\tilde{x},\tilde{y},\tilde{z}) + \delta^2\tilde{c}_2^o(\tilde{x},\tilde{y},\tilde{z}) + \cdots, \tag{25b}$$

where we used superscript o to label the outer solution and subscripts $1,2,\ldots$ to identify the unknown summands in the asymptotic expansions (see, for example, [37]). A consistent notation is used for the asymptotic expansions of the inner solutions.

By substituting Eq. (25) into the governing Eqs. (21a) and (21b), using the boundary conditions (24b), and equating terms of the same order, we obtain an hierarchy of partial differential equations for $\tilde{\psi}_0^o, \tilde{\psi}_1^o, \ldots$ and $\tilde{c}_0^o, \tilde{c}_1^o, \ldots$. At the leading order, we find the following concentration and charge distribution in the bulk region:

$$\tilde{c}_0^o(\tilde{x},\tilde{y},\tilde{z}) = 1, \tag{26a}$$

$$\tilde{\psi}_0^o(\tilde{x},\tilde{y},\tilde{z}) = A, \tag{26b}$$

where A is a constant parameter that represents the electric potential in the polymer bulk. The constant A is an unknown that is determined by matching between the outer and inner solutions.

B. Inner expansions: Electrode-polymer interfaces

In order to determine valid expansions for the concentration and electric potential in the vicinity of the electrodes, we magnify the boundary layers' depth by defining the stretching transformations

$$\xi^{\pm}(\tilde{x},\tilde{y},\tilde{z}) = \frac{1}{\delta\sqrt{\tilde{J}^{\pm}(\tilde{y},\tilde{z})}}[1 - \tilde{\rho}^{\pm}(\tilde{y},\tilde{z}) \mp \tilde{x}]. \tag{27}$$

The stretching transformations (27) are needed to magnify the boundary layer extent in the vicinity of the anode and cathode, that is, for $\tilde{x}$ in the neighborhood of $\pm[1 - \rho^{\pm}(\tilde{y},\tilde{z})]$.

We define the functions $\tilde{c}^{\pm}$ and $\tilde{\psi}^{\pm}$ such that

$$\tilde{c}^{\pm}(\xi^{\pm}(\tilde{x},\tilde{y},\tilde{z}),\tilde{y},\tilde{z}) = \tilde{c}(\tilde{x},\tilde{y},\tilde{z}), \tag{28a}$$

$$\tilde{\psi}^{\pm}(\xi^{\pm}(\tilde{x},\tilde{y},\tilde{z}),\tilde{y},\tilde{z}) = \tilde{\psi}(\tilde{x},\tilde{y},\tilde{z}). \tag{28b}$$

By using the chain rule of differentiation, we find that the spatial derivatives of $\tilde{\psi}$ can be rewritten as

$$\frac{\partial\tilde{\psi}(\tilde{x},\tilde{y},\tilde{z})}{\partial\tilde{x}} = \mp\frac{1}{\delta\sqrt{\tilde{J}^{\pm}(\tilde{y},\tilde{z})}}\frac{\partial\tilde{\psi}^{\pm}(\xi^{\pm},\tilde{y},\tilde{z})}{\partial\xi^{\pm}}\bigg|_{\xi^{\pm}=\xi^{\pm}(\tilde{x},\tilde{y},\tilde{z})}, \tag{29a}$$

$$\tilde{\nabla}_s\tilde{\psi}(\tilde{x},\tilde{y},\tilde{z}) = \left(\tilde{\nabla}_s\tilde{\psi}^{\pm}(\xi^{\pm},\tilde{y},\tilde{z}) - \frac{\xi^{\pm}\tilde{\nabla}_s\tilde{J}^{\pm}(\tilde{y},\tilde{z})}{2\tilde{J}^{\pm}(\tilde{y},\tilde{z})}\frac{\partial\tilde{\psi}^{\pm}(\xi^{\pm},\tilde{y},\tilde{z})}{\partial\xi^{\pm}} - \frac{\tilde{\nabla}_s\tilde{\rho}^{\pm}(\tilde{y},\tilde{z})}{\delta\sqrt{\tilde{J}^{\pm}(\tilde{y},\tilde{z})}}\frac{\partial\tilde{\psi}^{\pm}(\xi^{\pm},\tilde{y},\tilde{z})}{\partial\xi^{\pm}}\right)\bigg|_{\xi^{\pm}=\xi^{\pm}(\tilde{x},\tilde{y},\tilde{z})}. \tag{29b}$$

An equivalent expression can be computed for the gradient of $\tilde{c}$ in terms of $\tilde{c}^{\pm}$.

The stretching transformations in Eq. (27) remove the singular perturbation in the Poisson equation (21a). Thus, we seek regular asymptotic expansions of the electric potential and concentration in the inner regions, that is,

$$\tilde{\psi}^{\pm}(\xi^{\pm},\tilde{y},\tilde{z}) = \tilde{\psi}_0^{\pm}(\xi^{\pm},\tilde{y},\tilde{z}) + \delta\tilde{\psi}_1^{\pm}(\xi^{\pm},\tilde{y},\tilde{z}) + \delta^2\tilde{\psi}_2^{\pm}(\xi^{\pm},\tilde{y},\tilde{z}) + \cdots, \tag{30a}$$

$$\tilde{c}^{\pm}(\xi^{\pm},\tilde{y},\tilde{z}) = \tilde{c}_0^{\pm}(\xi^{\pm},\tilde{y},\tilde{z}) + \delta\tilde{c}_1^{\pm}(\xi^{\pm},\tilde{y},\tilde{z}) + \delta^2\tilde{c}_2^{\pm}(\xi^{\pm},\tilde{y},\tilde{z}) + \cdots. \tag{30b}$$

By substituting the inner expansions (30) into the governing Eq. (21), we obtain an hierarchy of partial differential equations for the asymptotic sequences of $\tilde{\psi}^+$, $\tilde{\psi}^-$, $\tilde{c}^+$, and $\tilde{c}^-$. At the leading order, we find

$$\frac{\partial^2\tilde{\psi}_0^{\pm}(\xi^{\pm},\tilde{y},\tilde{z})}{\partial(\xi^{\pm})^2} = 1 - \tilde{c}_0^{\pm}(\xi^{\pm},\tilde{y},\tilde{z}), \tag{31a}$$

$$\frac{\partial\tilde{c}_0^{\pm}(\xi^{\pm},\tilde{y},\tilde{z})}{\partial\xi^{\pm}} + \tilde{c}_0^{\pm}(\xi^{\pm},\tilde{y},\tilde{z})[1 - \nu\tilde{c}_0^{\pm}(\xi^{\pm},\tilde{y},\tilde{z})]\frac{\partial\tilde{\psi}_0^{\pm}(\xi^{\pm},\tilde{y},\tilde{z})}{\partial\xi^{\pm}} = 0. \tag{31b}$$

Since the inner expansions are valid at the electrode-polymer interfaces, they should satisfy the boundary conditions (24a) that, at the leading order, yields

$$\tilde{\psi}_0^{\pm}(0,\tilde{y},\tilde{z}) = \pm \frac{\alpha}{2}. \tag{32}$$

Moreover, the inner expansions should satisfy the integral constraint (24c) that, at the leading order, gives

$$-\int_{\tilde{S}} \sqrt{\tilde{J}^+(\tilde{y},\tilde{z})} \frac{\partial \tilde{\psi}_0^+(0,\tilde{y},\tilde{z})}{\partial \xi^+} d\tilde{S} = \int_{\tilde{S}} \sqrt{\tilde{J}^-(\tilde{y},\tilde{z})} \frac{\partial \tilde{\psi}_0^-(0,\tilde{y},\tilde{z})}{\partial \xi^-} d\tilde{S}. \tag{33}$$

Similarly, at the leading order, the dimensional charge and bending moment in Eqs. (15) and (20) become

$$Q = -\frac{Fc_0\lambda h^2}{|\mathcal{S}|} \int_{\tilde{S}} \sqrt{\tilde{J}^+(\tilde{y},\tilde{z})} \frac{\partial \tilde{\psi}_0^+(0,\tilde{y},\tilde{z})}{\partial \xi^+} d\tilde{S}, \tag{34a}$$

$$M = 2khQ + Fc_0\lambda h^3 \int_{\tilde{S}} \left(\tilde{\rho}^+(\tilde{y},\tilde{z}) \sqrt{\tilde{J}^+(\tilde{y},\tilde{z})} \frac{\partial \tilde{\psi}_0^+(0,\tilde{y},\tilde{z})}{\partial \xi^+} - \tilde{\rho}^-(\tilde{y},\tilde{z}) \sqrt{\tilde{J}^-(\tilde{y},\tilde{z})} \frac{\partial \tilde{\psi}_0^-(0,\tilde{y},\tilde{z})}{\partial \xi^-} \right) d\tilde{S}. \tag{34b}$$

We note that the first summand in Eq. (20) does not appear in the leading-order expansion of the average bending moment since it is proportional to δ^2, while the other two summands are proportional to δ.

C. Matching

Matching between the outer solution and the inner solutions is obtained by enforcing the following set of equalities:

$$\lim_{\xi^{\pm}\to\infty} \tilde{c}^{\pm}(\xi^{\pm},\tilde{y},\tilde{z}) = \lim_{\tilde{x}\to\pm(1-\rho^{\pm}(\tilde{y},\tilde{z}))} \tilde{c}^o(\tilde{x},\tilde{y},\tilde{z}), \tag{35a}$$

$$\lim_{\xi^{\pm}\to\infty} \tilde{\psi}^{\pm}(\xi^{\pm},\tilde{y},\tilde{z}) = \lim_{\tilde{x}\to\pm(1-\rho^{\pm}(\tilde{y},\tilde{z}))} \tilde{\psi}^o(\tilde{x},\tilde{y},\tilde{z}). \tag{35b}$$

By specializing Eq. (35) to the leading order and by using Eq. (26), we find the following conditions on the inner solutions:

$$\lim_{\xi^{\pm}\to\infty} \tilde{c}_0^{\pm}(\xi^{\pm},\tilde{y},\tilde{z}) = 1, \tag{36a}$$

$$\lim_{\xi^{\pm}\to\infty} \tilde{\psi}_0^{\pm}(\xi^{\pm},\tilde{y},\tilde{z}) = A. \tag{36b}$$

The inner solutions for the concentration and the electric potential along with the electric potential A in the bulk polymer region are determined by solving Eq. (31) subjected to conditions (32), (33), and (36b).

D. Composite solution

At the leading order, the concentration and electric field distribution in the whole polymer region are determined by combining the outer solution in Eq. (26) with the inner solutions $\tilde{c}_0^{\pm}$ and $\tilde{\psi}_0^{\pm}$ and by accounting for their common limit condition (36). More specifically, the concentration and electric potential in the polymer at the leading order are given by

$$\tilde{c}_0(\tilde{x},\tilde{y},\tilde{z}) = -1 + \tilde{c}_0^+\left(\frac{1-\tilde{\rho}^+(\tilde{y},\tilde{z})-\tilde{x}}{\delta\sqrt{\tilde{J}^+(\tilde{y},\tilde{z})}},\tilde{y},\tilde{z} \right) + \tilde{c}_0^-\left(\frac{1-\tilde{\rho}^-(\tilde{y},\tilde{z})+\tilde{x}}{\delta\sqrt{\tilde{J}^-(\tilde{y},\tilde{z})}},\tilde{y},\tilde{z} \right), \tag{37a}$$

$$\tilde{\psi}_0(\tilde{x},\tilde{y},\tilde{z}) = -A + \tilde{\psi}_0^+\left(\frac{1-\tilde{\rho}^+(\tilde{y},\tilde{z})-\tilde{x}}{\delta\sqrt{\tilde{J}^+(\tilde{y},\tilde{z})}},\tilde{y},\tilde{z} \right) + \tilde{\psi}_0^-\left(\frac{1-\tilde{\rho}^-(\tilde{y},\tilde{z})+\tilde{x}}{\delta\sqrt{\tilde{J}^-(\tilde{y},\tilde{z})}},\tilde{y},\tilde{z} \right). \tag{37b}$$

E. Leading-order solution of the inner problems

In order to reduce the order of the nonlinear boundary value problem (21), we introduce the functions $\eta^{\pm}$ such that

$$\tilde{c}_0^{\pm} = \frac{\exp(\eta^{\pm})}{1-\nu+\nu\exp(\eta^{\pm})}. \tag{38}$$

By substituting Eq. (38) into Eq. (31b), we have

$$\frac{\partial \eta^{\pm}(\xi^{\pm},\tilde{y},\tilde{z})}{\partial \xi^{\pm}} + \frac{\partial \tilde{\psi}_0^{\pm}(\xi^{\pm},\tilde{y},\tilde{z})}{\partial \xi^{\pm}} = 0 \tag{39}$$

that implies

$$\eta^{\pm}(\xi^{\pm},\tilde{y},\tilde{z}) = -\tilde{\psi}_0^{\pm}(\xi^{\pm},\tilde{y},\tilde{z}) + K^{\pm}(\tilde{y},\tilde{z}), \tag{40}$$

where $K^{\pm}$ are unknown functions that are independent of the stretched variables.

By substituting Eqs. (38) and (40) into Eq. (31a), we find two second-order nonlinear ordinary differential equations in the $\xi^{\pm}$ variables for the functions $\eta^{\pm}(\xi^{\pm},\tilde{y},\tilde{z})$. That is, we find

$$\frac{\partial^2 \eta^{\pm}(\xi^{\pm},\tilde{y},\tilde{z})}{\partial(\xi^{\pm})^2} = f(\eta^{\pm}(\xi^{\pm},\tilde{y},\tilde{z})), \tag{41}$$

where the nonlinear function f is defined by

$$f(\eta) = \frac{\exp(\eta)}{1-\nu+\nu\exp(\eta)} - 1. \tag{42}$$

Boundary conditions for $\eta^{\pm}(\xi^{\pm},\tilde{y},\tilde{z})$ and subsidiary conditions for the introduced parameter A and the functions $K^{\pm}$ are obtained by substituting Eq. (38) into the boundary conditions (32), the matching conditions (35a) and (35b), and the integral condition (33). By following this procedure, we find

$$\eta^{\pm}(0,\tilde{y},\tilde{z}) = K^{\pm}(\tilde{y},\tilde{z}) \mp \frac{\alpha}{2}, \tag{43a}$$

$$\lim_{\xi^{\pm}\to\infty} \eta^{\pm}(\xi^{\pm},\tilde{y},\tilde{z}) = 0, \tag{43b}$$

$$\lim_{\xi^{\pm}\to\infty} \eta^{\pm}(\xi^{\pm},\tilde{y},\tilde{z}) = K^{\pm}(\tilde{y},\tilde{z}) - A, \tag{43c}$$

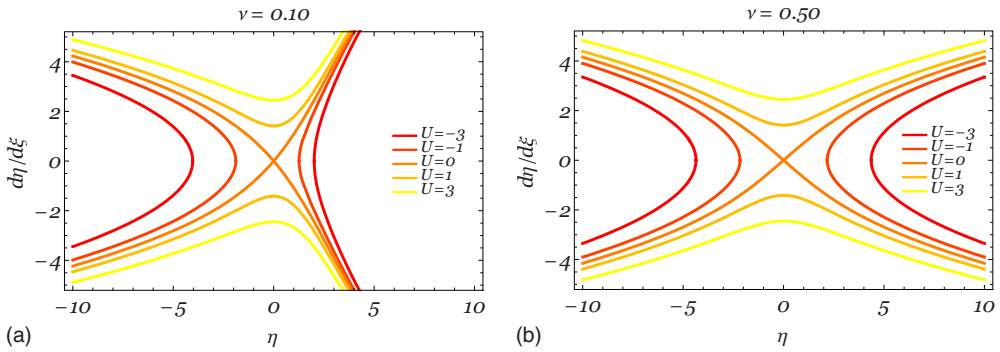

FIG. 2. (Color online) Level curves of Eq. (44) for two different values of the parameter ν.

$$+\int_{\tilde{S}}\sqrt{\tilde{J}^{+}(\tilde{y},\tilde{z})}\left.\frac{\partial\eta^{+}(\xi^{+},\tilde{y},\tilde{z})}{\partial\xi^{+}}\right|_{\xi^{+}=0}d\tilde{S}$$

$$=-\int_{\tilde{S}}\sqrt{\tilde{J}^{-}(\tilde{y},\tilde{z})}\left.\frac{\partial\eta^{-}(\xi^{-},\tilde{y},\tilde{z})}{\partial\xi^{-}}\right|_{\xi^{-}=0}d\tilde{S}. \quad (43d)$$

From Eqs. (43b) and (43c), we have that $K^{\pm}$ are constants and both equal to the parameter A. The functions $\eta^{\pm}$ and the parameter A are determined by solving the nonlinear second-order ordinary differential equation (41) in the $\xi^{\pm}$ variables subjected to conditions (43a), (43b), and (43d).

The problem can be further simplified and transformed into a manageable Cauchy problem by a close analysis of Eq. (41). More specifically, we note that the function

$$U\left(\eta,\frac{d\eta}{d\xi}\right)=\frac{1}{2}\left(\frac{d\eta}{d\xi}\right)^{2}+\eta-\ln\left\{\frac{1}{\nu}[(1-\nu)+\nu\exp(\eta)]\right\} \quad (44)$$

is a first integral of

$$\frac{d^{2}\eta(\xi)}{d\xi^{2}}=f(\eta). \quad (45)$$

By making use of the first integral U, we transform the nonlinear boundary value problem (41) into an initial value problem. A similar approach has been used in [23] to analyze charge dynamics of IPMCs with flat electrodes in absence of steric effects. In Fig. 2, we show the level lines of U in the phase plane for two selected values ν.

From Fig. 2, we evince that the only solutions of Eq. (45) that tend to the origin as ξ goes to infinity are those for which $U=0$ that are in the second and fourth quadrants of the phase plane. Therefore, we replace the limit conditions (43b) with

$$U\left(\eta^{\pm},\frac{\partial\eta^{\pm}}{\partial\xi^{\pm}}\right)=0, \quad (46)$$

along with the constraint that the solution is in the second or fourth quadrant of the phase plane, that is,

$$\frac{\partial\eta^{\pm}(\xi^{\pm},\tilde{y},\tilde{z})}{\partial\xi^{\pm}}\eta^{\pm}(\xi^{\pm},\tilde{y},\tilde{z})<0. \quad (47)$$

By combining (43a), (43d), (46), and (47) and assuming that $\alpha>0$, we determine the initial conditions of the Cauchy problem in terms of the unknown constant A, that is, we find

$$\left.\frac{\partial\eta^{+}(\xi^{+},\tilde{y},\tilde{z})}{\partial\xi^{+}}\right|_{\xi^{+}=0}=\vartheta\left(A-\frac{\alpha}{2}\right), \quad (48a)$$

$$\left.\frac{\partial\eta^{-}(\xi^{-},\tilde{y},\tilde{z})}{\partial\xi^{-}}\right|_{\xi^{-}=0}=-\vartheta\left(A+\frac{\alpha}{2}\right), \quad (48b)$$

where A is the root of the transcendental equation

$$\vartheta\left(A+\frac{\alpha}{2}\right)|\tilde{S}^{+}|=\vartheta\left(A-\frac{\alpha}{2}\right)|\tilde{S}^{-}| \quad (49)$$

in the interval $(-\alpha/2,\alpha/2)$ and

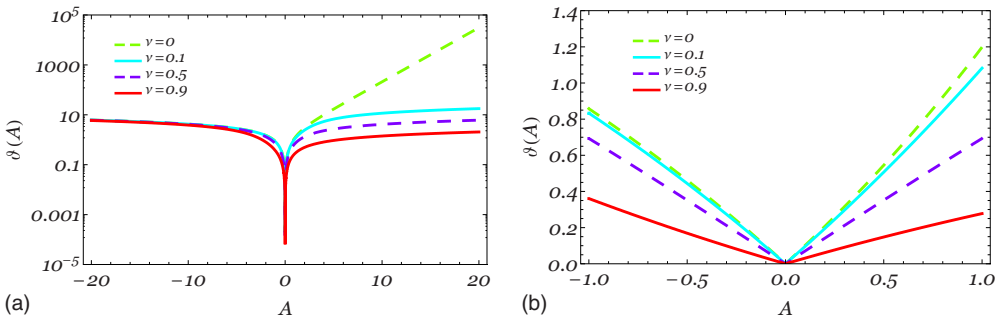

FIG. 3. (Color online) ϑ as a function of the bulk polymer potential A for different values of the packing parameter ν: (a) large parameter variation in logarithmic scale and (b) detailed plot in the neighborhood of the origin.

$$\vartheta(A) = \sqrt{2}\sqrt{-A + \frac{1}{\nu}\ln[1-\nu+\nu\exp(A)]}. \quad (50)$$

We note that the numerical value of the bulk potential A depends only on the ratio between the overall electrodes' surface area and the packing parameter ν.

Figure 3 shows the function ϑ for different values of the packing parameter ν. The function ϑ increases as the absolute value of A increases for any value of ν. The rate of change in ϑ increases as ν increases and is larger for positive values of A as compared to negative values of A.

Once the constant A is determined from Eq. (49), all the initial conditions of the Cauchy problem in Eqs. (43a) and (48) can be computed. Thus, Eq. (45) can be numerically integrated to determine the functions $\eta^{\pm}$. The concentration and electric potential in the whole IPMC region are computed from the knowledge of the constant A and the functions $\eta^{\pm}$ by using Eqs. (38) and (40) and recalling that $K^{\pm}(\tilde{y},\tilde{z})=A$.

The charge per unit nominal surface stored in the IPMC is computed by using Eqs. (40) and (48) in Eq. (34a), that is,

$$Q = Fc_0\lambda\frac{|\mathcal{S}^+|}{|\mathcal{S}|}\vartheta\left(A-\frac{\alpha}{2}\right), \quad (51)$$

where A is the solution of Eq. (49). From Eq. (51), we note that the charge stored in the IPMC is independent of the IPMC thickness and increases linearly with the electrode surface area.

The differential capacitance of the IPMC per unit nominal surface area is defined as the rate of change in the stored charge as a function of the applied voltage divided by the nominal IPMC surface, that is,

$$\gamma = \frac{dQ}{dV} = \frac{\varepsilon_0\varepsilon_r}{\lambda}\frac{|\mathcal{S}^+|}{|\mathcal{S}|}\left.\frac{d\vartheta\left(A-\frac{\alpha}{2}\right)}{d\alpha}\right|_{\alpha=FV/RT}. \quad (52)$$

The average bending moment of the IPMC is computed by using Eqs. (40) and (48) in Eq. (34b) and by accounting for Eq. (5), that is,

$$M = 2khQ = 2khFc_0\lambda\frac{|\mathcal{S}^+|}{|\mathcal{S}|}\vartheta\left(A-\frac{\alpha}{2}\right). \quad (53)$$

We note that Eq. (53) indicates that the charge stored in the IPMC and its bending moment are linearly related in accordance with the experimental results in [33].

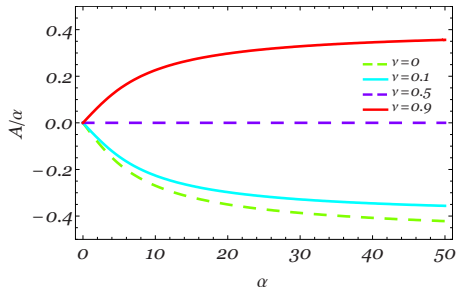

FIG. 4. (Color online) Relative bulk potential as a function of the applied potential for equal surface area electrodes.

IV. RESULTS

A. Bulk potential

If the anode and cathode have the same surface area, that is, $|\tilde{\mathcal{S}}^-|=|\tilde{\mathcal{S}}^+|$, Eq. (49) can be solved to yield the following simple expression for A:

$$A = \ln\left(\frac{1-\nu}{\nu}\frac{\sinh\left(\frac{\alpha\nu}{2}\right)}{\sinh\left(\frac{\alpha(1-\nu)}{2}\right)}\right). \quad (54)$$

In addition, in the limit of $\nu\to 0$, we have $A=\ln\{\alpha/[2\sinh(\alpha/2)]\}$. We note that in case of flat electrodes $|\tilde{\mathcal{S}}^-|=|\tilde{\mathcal{S}}^+|=1$. Figure 4 shows the relative bulk potential as a function of the applied voltage for different values of the packing parameter in the case the two electrodes have the same surface area. For small applied voltages, the bulk potential is approximately zero for any value of ν. As the applied voltage increases, the relative bulk potential monotonically approaches $\nu-1/2$. The sign of the bulk potential for high values of α depends on the packing parameter. For $\nu<1/2$, the bulk potential is negative, whereas, for $\nu>1/2$, it is positive. For $\nu=1/2$, the bulk potential is zero for any value of α.

Figure 5 shows the relative bulk potential for unequal electrodes as a function of the packing parameter ν for $\alpha=1$ and $\alpha=10$. The bulk potential is determined by solving Eq. (49). If the cathode area is larger than the anode area, the bulk potential is higher than the one obtained in case of equal surface area electrodes. On the other hand, if the cathode area is smaller than the anode area, the bulk potential tends to be smaller than the one in case of flat electrodes. As the

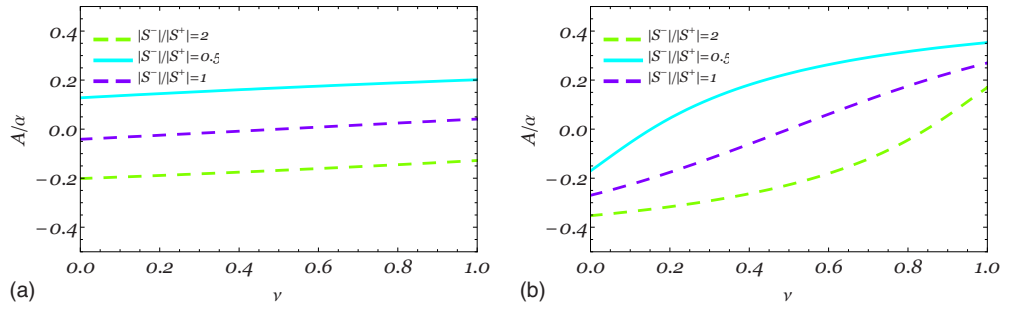

FIG. 5. (Color online) Relative bulk potential for unequal surface electrodes and (a) $\alpha=1$ and (b) $\alpha=10$.

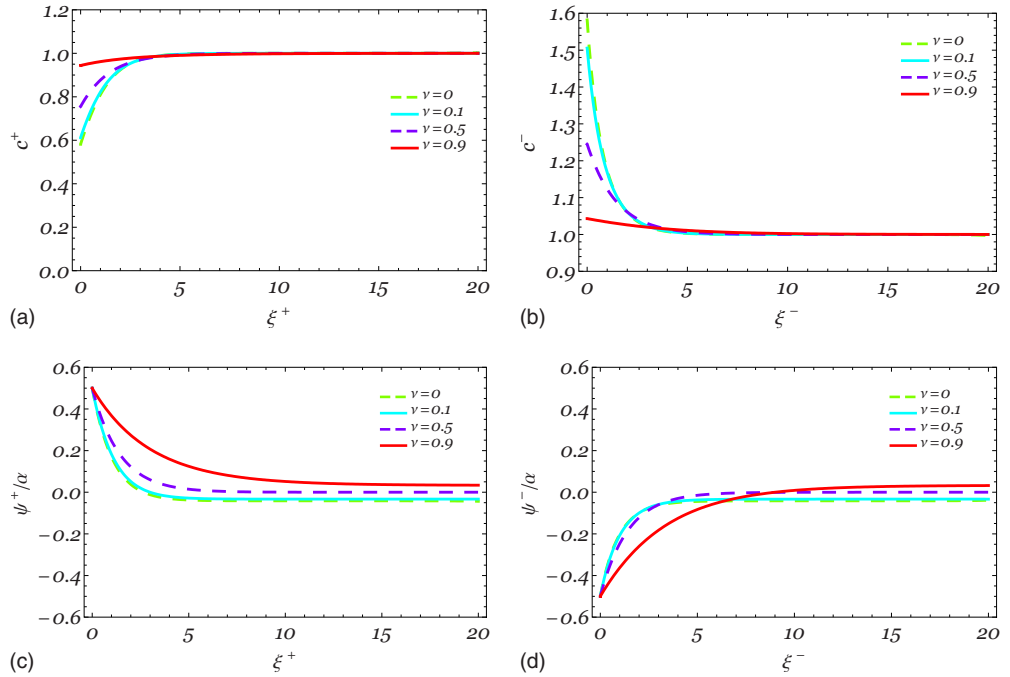

FIG. 6. (Color online) Concentration and relative electric potential in the proximity to the electrodes at $\alpha=1$.

applied voltage increases, the dependence of the relative bulk potential on the packing parameter becomes remarkably nonlinear.

B. Concentration and electric potential profiles

Figures 6 and 7 show the boundary layers in the concentration and relative potential for $\alpha=1$ and $\alpha=10$ and different values of the packing parameter ν in case of equal surface electrodes. We note that the stretching variable depends on the local surface area of the electrode. Therefore, for a given value of $\xi^{\pm}$, the actual distance from the electrode surface decreases as the electrode surface increases.

Depletion of mobile counterions at the polymer-anode interface and mobile counterion enrichment at the polymer-cathode interface is affected by both the applied potential α and the packing parameter ν. For a given applied voltage, these phenomena are more prominent for smaller values of ν. Indeed, at larger values of the packing parameter ν, redistribution of mobile counterions in the IPMC is limited. For a

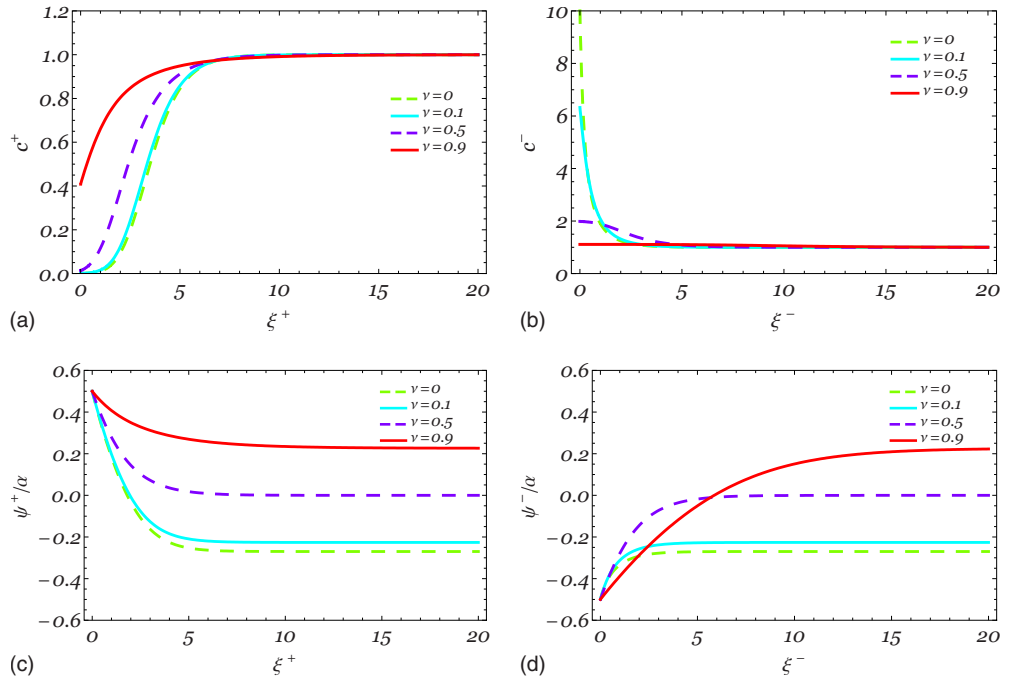

FIG. 7. (Color online) Concentration and relative electric potential in the proximity to the electrodes at $\alpha=10$.

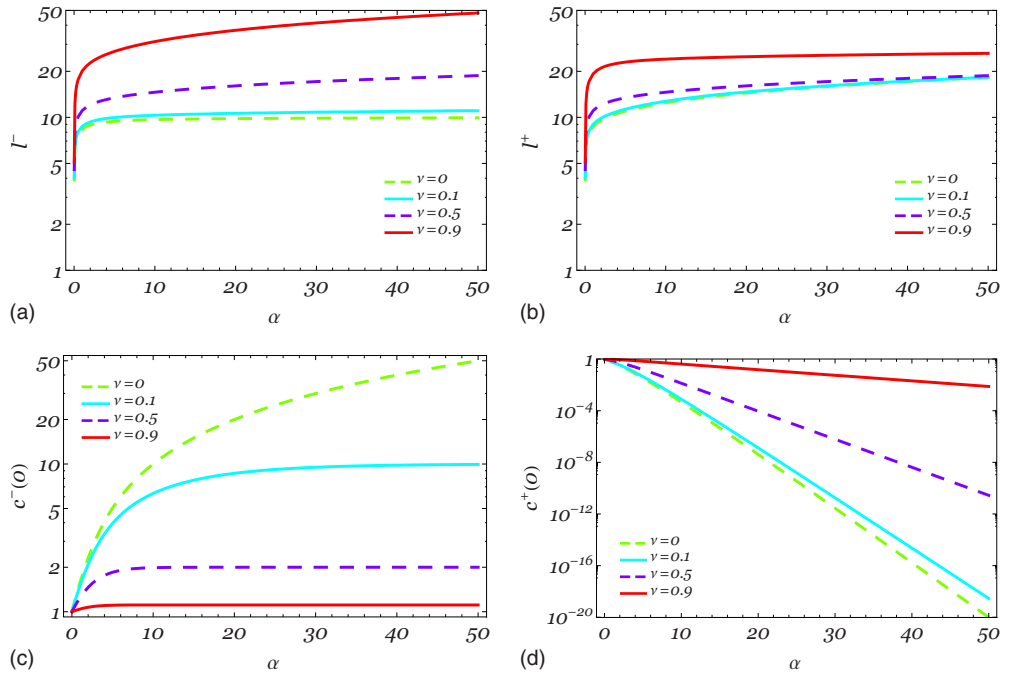

FIG. 8. (Color online) Extent of concentration boundary layers in the proximity to (a) the anode and (b) cathode and numerical values of the concentration values at (c) the anode and (d) cathode.

given packing parameter ν, increasing the applied electric potential results into severe asymmetries in the concentration distribution at the polymer-electrode interfaces. For small values of α, the concentration is approximately an antisymmetric function of the through-the-thickness variable $\tilde{x}$. As the applied potential increases, the concentration at the two polymer-electrode interfaces becomes remarkably different and presents steep growth in the vicinity of the cathode and flat reduction in the anode proximity.

The profile of the relative electric potential in the vicinity of the electrodes is also affected by both the applied voltage and the packing parameter. For small values of α, the relative potential is approximately antisymmetric with respect to the coordinate $\tilde{x}$ and the bulk potential is approximately zero. As the potential increases, the bulk potential becomes remarkably different than zero and the potential distribution loses the antisymmetry with respect to $\tilde{x}$. The bulk potential A as a function of ν and α follows the trend illustrated in Fig. 4.

For given electrodes, the extent of the boundary layers and the concentration profile in the proximity of the electrodes depend on both the applied voltage and the packing parameter ν. For two equal surface electrodes, Figs. 8(a) and 8(b) illustrate the extents of the boundary layers, say $l^{\pm}$, in the range $\alpha=0.01-50$ and for different values of ν. The boundary layers' extent is arbitrarily defined as the value of the stretched variable at which the concentration is within 10^{-4} of its bulk value, that is, $c^+>0.9999$ and $c^-<1.0001$. The boundary layers' depth sensibly increases as the packing parameter ν increases due to steric effects that force the counterions to occupy a more extended region in the cathode proximity. For small values of ν, the concentration boundary layers' extent rapidly reaches a saturation value as the potential applied across the electrodes increases, whereas for high values of ν a continuous growth of boundary layers' extent is observed in the studied range of α. For the same range of parameters, Figs. 8(c) and 8(d) show the concentration at the anode and cathode, respectively, for different values of α and ν. We note that as the voltage applied across the electrodes increases, the counterion concentration at the cathode increases while it decreases at the anode. These changes are controlled by the parameter ν. In particular, we note that, for $\nu\neq 0$, all the concentrations achieve their packing limit $1/\nu$ in the cathode proximity for large values of α.

As made clear by Figs. 8(a) and 8(b), the dimensionless boundary layer extent is on the order of 10. Thus, the dimensional thickness in the x direction of the concentration boundary layers is approximately a few tens of $\lambda\sqrt{J^{\pm}(y,z)}$. For the leading-order solution to be valid, this depth needs to be smaller than the in-plane characteristic length of the rough electrodes. For example, for a sinusoidal surface roughness modeled by $\tilde{\rho}^{\pm}=\epsilon\sin(2\pi y/\ell_y)\sin(2\pi z/\ell_z)$, we may reasonably require that $100\lambda\sqrt{1+(2\pi\epsilon/\min\{\ell_y,\ell_z\})^2}<\min\{\ell_y,\ell_z\}$. For $\lambda\approx 0.1-1$ nm and $\ell_y=\ell_z=\epsilon$, we may thus infer that the smallest roughness length scale that the Debye screening length resolves is in the range of 50–500 nm. In other words, the scale that should be used to measure the surface roughness of IPMC electrodes should be on the order of 50–500 nm that is well in line with experimentally observed length scales of metal protrusions observed in IPMCs [30,31,33].

C. Stored charge and bending moment

Figure 9 displays the function $\vartheta(A-\alpha/2)$ and its derivative as a function of α for equal surface electrodes. These functions fully define the dependence of the stored charge, capacitance, and bending moment on the applied voltage V [see Eqs. (51)–(53)]. For small applied voltages and $\nu=0$, the IPMC capacitance is equal to $(\varepsilon_0\varepsilon_r|\mathcal{S}^+|)/(2\lambda|\mathcal{S}|)$ which cor-

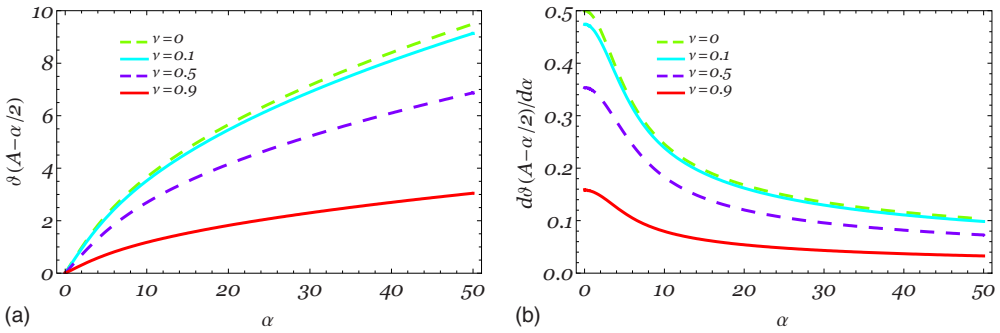

FIG. 9. (Color online) Nondimensional functions defining the overall IPMC response as the applied voltage increases, according to Eqs. (51)–(53).

responds to the series connection of two equal double-layer capacitances in the proximity of the electrodes. As ν increases, the capacitance reduces due to the packing of counterions in the proximity of the cathode. For typical IPMCs (see, for example, [2,5,20,30,31,33]), $(\varepsilon_0\varepsilon_r)/(2\lambda) \approx 0.1-1$ F m^{-2} and the capacitance per unit surface ranges in the interval of 10–1000 F m^{-2}. Therefore, the surface roughness is responsible for a capacitance boost of 1–4 orders of magnitude which is consistent with the morphological studies in [30–32]. As the voltage increases, the capacitance reduces due to the increase in the boundary layer thickness [see Figs. 8(a) and 8(b)]. Similarly, the bending moment and the stored charge decrease as the applied voltage increases. This nonlinear behavior has been experimentally observed in [20] for a cantilever IPMC strip subjected to different step-input voltages as discussed in what follows.

Figure 10 displays $\vartheta(A-\alpha/2)$ as a function of α for different values of the parameter ν and for $|\mathcal{S}^-|/|\mathcal{S}^+|=2$ and $|\mathcal{S}^-|/|\mathcal{S}^+|=0.5$. By comparing Figs. 9(a), 10(a), and 10(b) we note that differences in the electrode surface area drastically change the impact of the packing parameter on the IPMC charge and bending moment. In particular, as the cathode surface reduces as compared to the anode surface, the packing parameter severely reduces the charge stored in the IPMC. Indeed, reducing the cathode surface area limits the space available to the mobile charges and therefore enhances packing phenomena.

D. Comparison with experimental data

Here, we compare our modeling results with the experimental data on IPMC cantilever strips in [20]. Experimental data in [20] refer to an IPMC that includes Nafion-117 as the ion-exchange membrane, lithium as the counterion species, and formamide as the solvent with a nearly 100% weight uptake. The electrodes are composed of RuO_2 and a thin layer of gold. The approximate nominal thickness of the IPMC is 0.5 mm. Experiments are conducted at room temperature, that is, $T=293$ K. The nominal concentration of fixed charges at 100% formamide uptake is reported in [20] to be $c_0=1073$ mol m^{-3}.

From the experimental data reported in [20] for the stored charge density per unit IPMC nominal surface area versus the applied voltage, we identify the parameter $Fc_0\lambda|\mathcal{S}^+|/|\mathcal{S}|$ in Eq. (51) by setting $\nu=0$ and assuming that the electrodes have the same surface area. Figure 11(a) shows the experimental data versus the theoretical predictions from Eqs. (51) and (54) with $Fc_0\lambda|\mathcal{S}^+|/|\mathcal{S}|=198$ C m^{-2}. By selecting $\varepsilon_r=10$ consistently with the available data on the dielectric constant of formamide and Nafion, which are 84 and 3, respectively (see, for example, [16]), we find that $\lambda=1.45$ Å. In this case, the ratio of the electrode surface area versus the nominal surface area is found to be 13200. The packing parameter can be potentially identified from the morphology of the electrodes, that is, by setting the value of $|\mathcal{S}^+|/|\mathcal{S}|$ and identifying ν from the stored charge experiments. In this case, due to the lack of experimental data, we set $\nu=0$ and identify the electrode roughness.

Along with charge data, in [20], experimental data on IPMC bending strains are reported. By assuming that the bending strain induced in the IPMC is proportional to the average bending moment M through a proportionality constant κ, from Eq. (53), we have that $\chi=M/\kappa=(2kh/\kappa)Q$.

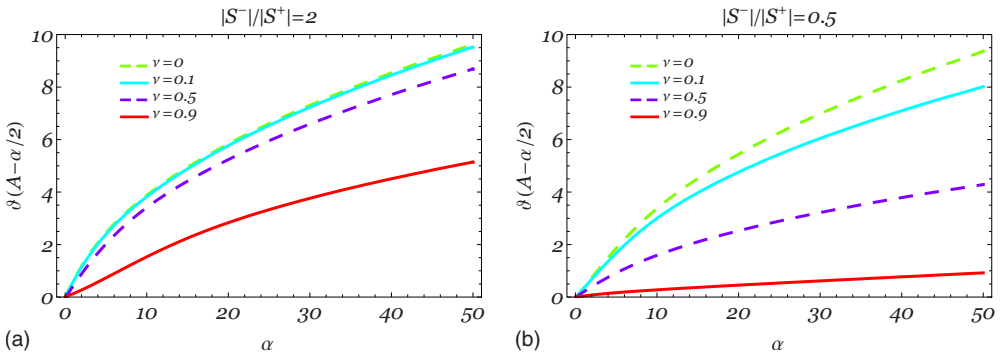

FIG. 10. (Color online) Dependence of the stored charge and bending moment on the applied voltage for (a) larger anode surface and (b) larger cathode surface.

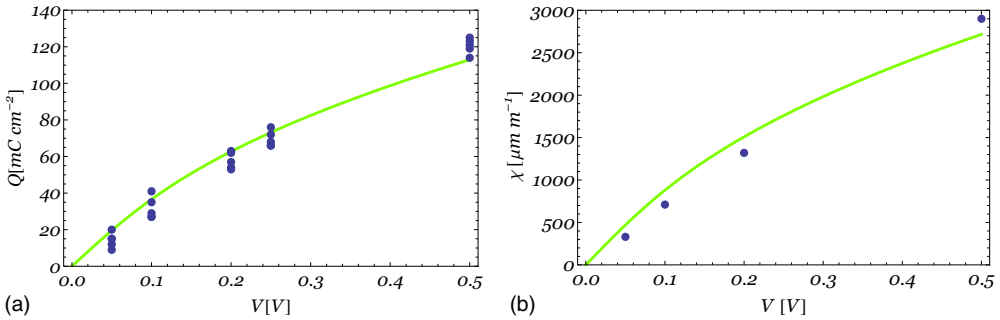

FIG. 11. (Color online) Comparison between the proposed analytical solution (solid line) and experimental results of [20] (dots): (a) stored charge per unit surface and (b) bending strain.

Therefore, the coefficient $2kh/\kappa$ can be experimentally identified by comparing the strain data with the identified values of the stored charge per unit surface area. Figure 11(b) displays the experimental data from [20] together with the predictions obtained by using the stored charge in Fig. 11(a) and $2kh/\kappa=2.4\times10^{-6}$ C^{-1} m^2. The proposed model predictions are in good agreement with the experimental results on bending strain. Superior data fitting may be possible by considering different electrode surfaces as well as packing phenomena, see Figs. 10(a) and 10(b), or nonlinear stress-charge constitutive behaviors, see [21]. Discrepancies between theory and experiments for the IPMC stored charge may be due to the experimental identification of the charge from the IPMC current that may be affected by redox reactions as discussed in [21].

V. CONCLUSIONS

We studied the influence of steric effects and electrode surface roughness on the nonlinear static electromechanical response of IPMCs. We used the modified Poisson-Nernst-Planck model proposed in [34,35] to describe the distribution of the electric potential and the concentration of mobile counterions in response to a static voltage difference applied across the IPMC electrodes. We used the method of matched asymptotic expansions to determine an analytical solution for the electric potential and the concentration of counterions in the whole IPMC domain. Further, we determined closed-form expressions for the charge stored in the IPMC and for its differential capacitance and bending moment production. We showed that bending moment production is proportionally related to charge storage in accordance with the experimental evidence reported in [33].

The analytical solution shows the formation of thin boundary layers in the proximity of the polymer-electrode interfaces. For positively charged counterions, the anode-polymer interface shows prominent counterion depletion, while remarkable counterion enrichment is present at the cathode-polymer interface. The boundary layer formation is controlled by the packing limit of the counterion concentration, the applied voltage across the IPMC electrodes, and the electrode surface roughness. As the surface area of the electrodes increases, a larger area becomes available for boundary layers development. Therefore, major increases in the charge, capacitance, and bending moment are observed in accordance with the experimental evidence reported in [30,31]. The charge stored in the IPMC and the produced bending moment nonlinearly increase as the applied voltage increases in striking agreement with the experimental results in [20]. Further, we analyzed the effect of unequal electrode surface area on the IPMC electromechanical response. We showed that unequal surface areas lead to remarkable asymmetries in the IPMC response as the cathode and anode are switched and that these asymmetries are enhanced by steric effects.

The proposed study does not consider chemical reactions and Stern layers at the polymer-electrode interfaces and is limited to the case of small Debye lengths based on the sole leading-order solution. Future work will be devoted to analyze the response of IPMCs in case of more complex physical scenarios at the polymer-electrode interfaces for a broad range of Debye screening lengths.

ACKNOWLEDGMENTS

This research was supported by the National Science Foundation under Grant No. CMMI-0745753. The author wishes to thank Nicole Abaid and Matteo Aureli for their careful review of the manuscript.

[1] K. Farinholt and D. J. Leo, Mech. Mater. **36**, 421 (2004).
[2] Z. Chen, X. Tan, A. Will, and C. Ziel, Smart Mater. Struct. **16**, 1477 (2007).
[3] C. Bonomo, L. Fortuna, P. Giannone, S. Graziani, and S. Strazzeri, Smart Mater. Struct. **17**, 015014 (2008).
[4] C. Bonomo, P. Brunetto, L. Fortuna, P. Giannone, S. Graziani, and S. Strazzeri, IEEE Sens. J. **8**, 1486 (2008).
[5] S. Nemat-Nasser, J. Appl. Phys. **92**, 2899 (2002).
[6] B.-K. Fang, M.-S. Ju, and C.-C. K. Lin, Sens. Actuators, A **137**, 321 (2007).
[7] G. Del Bufalo, L. Placidi, and M. Porfiri, Smart Mater. Struct. **17**, 045010 (2008).

[8] T. T. Nguyen, N. S. Goo, V. K. Nguyen, Y. Yoo, and S. Park, Sens. Actuators, A **141**, 640 (2008).
[9] S. Guo, T. Fukuda, and K. Asaka, IEEE/ASME Trans. Mechatron. **8**, 136 (2003).
[10] B. Kim, D.-H. Kim, J. Jung, and J.-O. Park, Smart Mater. Struct. **14**, 1579 (2005).
[11] K. J. Kim, W. Yim, J. W. Paquette, and D. Kim, J. Intell. Mater. Syst. Struct. **18**, 123 (2007).
[12] E. Mbemmo, Z. Chen, S. Shatara, and X. Tan, *Modeling of biomimetic robotic fish propelled by an ionic polymer-metal composit acutator*, Proceedings of the 2008 IEEE International Conference on Robotics and Automation, (IEEE, Pasadena, CA, 2008), pp. 689–694.
[13] J. Brufau-Penella, M. Puig-Vidal, P. Giannone, S. Graziani, and S. Strazzeri, Smart Mater. Struct. **17**, 015009 (2008).
[14] R. Tiwari, K. Kim, and S. Kim, Smart Structures and Systems **4**, 549 (2008).
[15] P. G. de Gennes, K. Okumura, M. Shahinpoor, and K. J. Kim, Europhys. Lett. **50**, 513 (2000).
[16] S. Nemat-Nasser and J. Y. Li, J. Appl. Phys. **87**, 3321 (2000).
[17] P. J. Costa Branco and J. A. Dente, Smart Mater. Struct. **15**, 378 (2006).
[18] M. Porfiri, Smart Mater. Struct. **18**, 015016 (2009).
[19] T. Wallmersperger, B. Kroplin, and R. W. Gulch, Mech. Mater. **36**, 411 (2004).
[20] T. Wallmersperger, D. J. Leo, and C. S. Kothera, J. Appl. Phys. **101**, 024912 (2007).
[21] T. Wallmersperger, B. J. Akle, D. J. Leo, and B. Kroplin, Compos. Sci. Technol. **68**, 1173 (2008).
[22] K. Farinholt and D. J. Leo, J. Appl. Phys. **104**, 014512 (2008).
[23] M. Porfiri, J. Appl. Phys. **104**, 104915 (2008).
[24] M. Shahinpoor and K. J. Kim, Smart Mater. Struct. **13**, 1362 (2004).
[25] A. J. Bard and L. R. Faulkner, *Electrochemical Methods: Fundamentals and Applications* (John Wiley and Sons, Inc., Hoboken, NJ, 2001).
[26] L. I. Daikhin, A. A. Kornyshev, and M. Urbakh, Phys. Rev. E **53**, 6192 (1996).
[27] L. I. Daikhin, A. A. Kornyshev, and M. Urbakh, J. Chem. Phys. **108**, 1715 (1998).
[28] R. Guidelli and W. Schmickler, Electrochim. Acta **45**, 2317 (2000).
[29] G. Palasantzas and G. M. E. A. Backx, J. Chem. Phys. **118**, 4631 (2003).
[30] K. Onishi, S. Sewa, K. Asaka, N. Fujiwara, and K. Oguro, Electrochim. Acta **46**, 737 (2000).
[31] K. Onishi, S. Sewa, K. Asaka, N. Fujiwara, and K. Oguro, Electrochim. Acta **46**, 1233 (2001).
[32] S. J. Kim, S.-M. Kim, K. J. Kim, and Y. H. Kim, Smart Mater. Struct. **16**, 2286 (2007).
[33] B. J. Akle, D. J. Leo, M. A. Hickner, and J. E. McGrath, J. Mater. Sci. **40**, 3715 (2005).
[34] M. S. Kilic, M. Z. Bazant, and A. Ajdari, Phys. Rev. E **75**, 021502 (2007).
[35] M. S. Kilic, M. Z. Bazant, and A. Ajdari, Phys. Rev. E **75**, 021503 (2007).
[36] M. Van Dyke, *Perturbation Methods in Fluid Mechanics* (The Parabolic Press, Stanford, CA, 1975).
[37] A. H. Nayfeh, *Introduction to Perturbation Techniques* (Wiley-Interscience, New York, 1981).
[38] I. V. Andrianov and L. I. Manevitch, *Asymptotic Approaches in Nonlinear Dynamics* (Sprinder-Verlag, New York, NY, 1998).
[39] M. Z. Bazant, K. Thornton, and A. Ajdari, Phys. Rev. E **70**, 021506 (2004).
[40] Y. K. Suh and S. Kang, Phys. Rev. E **77**, 031504 (2008).
[41] N. Abaid, R. S. Eisenberg, and W. Liu, SIAM J. Appl. Dyn. Syst. **7**, 1507 (2008).
[42] J. N. Reddy, *Mechanics of Laminated Composite Plates and Shells: Theory and Analysis*, 2nd ed. (CRC Press, Boca Raton, FL, 2004).
[43] E. H. Mansfield, *The Bending and Stretching of Plates*, 2nd ed. (Cambridge University Press, New York, 1989).
[44] Z. Schuss, B. Nadler, and R. S. Eisenberg, Phys. Rev. E **64**, 036116 (2001).
[45] S.-H. Chung and S. Kuyucak, Biochim. Biophys. Acta **1565**, 267 (2002).